

# Adsorption of Metaldehyde by Oil Palm Kernel Biochar and Rice Husk Biochar: A Comparative Study

*Nur Salsabila Kamarudin*<sup>1,2</sup>, *Farrah Aini Dahalan*<sup>1,2,\*</sup>, *Muhammad Ikram Hakim Suhaimi*<sup>2</sup>, *Arina Azmina Ahmad Zubir*<sup>1,2</sup>, *Masitah Hasan*<sup>1,2</sup>, *Naimah Ibrahim*<sup>1,2</sup>, *Nabilah Aminah Lutpi*<sup>1,2</sup>, *Raja Nazrul Hakim Raja Nazri*<sup>3</sup> and *Nor Azizah Parmin*<sup>4</sup>

<sup>1</sup>Centre of Excellence for Water Research and Environmental Sustainability Growth (WAREG), Universiti Malaysia Perlis (UniMAP), 02600 Arau, Perlis, Malaysia

<sup>2</sup>Faculty of Civil Engineering Technology, Universiti Malaysia Perlis (UniMAP), 02600 Arau, Perlis, Malaysia

<sup>3</sup>Universiti Kuala Lumpur, Branch Campus Malaysian Institute of Chemical and Bioengineering Technology, Melaka, Malaysia

<sup>4</sup>Institute of Nano Electronic Engineering (INEE), Universiti Malaysia Perlis, Lot 106, 108 & 110, Blok A, Taman Pertiwi Indah, Jalan Kangar-Alor Setar, Seriab 01000 Kangar, Perlis, Malaysia

**Abstract.** Metaldehyde is a toxic molluscicide that has the potential to contaminate water supplies and damage aquatic life. Existing water treatment methods are ineffective at removing it from water bodies. In this study, oil palm kernel biochar (OPKB) and rice husk biochar (RHB) were utilized to assess metaldehyde adsorption. Using a batch adsorption approach, the physicochemical parameters of biochar and their metaldehyde adsorption capacities were investigated. The results indicated that the metaldehyde adsorption capacities of both varieties of biochar are significant. Considering the initial concentration of metaldehyde, contact time, and adsorbent dosages, OPKB demonstrated a higher metaldehyde adsorption capacity than RHB. The study examined metaldehyde's effects on OPKB and RHB using Langmuir and Freundlich isotherms. Both models provided a good fit, with the Freundlich model slightly better fitting. The study also used pseudo-first and second order kinetic models, revealing that the adsorption process follows pseudo-second-order kinetics for both biochar. This information can aid in developing efficient and successful metaldehyde removal technologies from contaminated water sources. This study showed that oil palm biochar has the potential to be an effective adsorbent for removing metaldehyde from contaminated water.

## 1 Introduction

Metaldehyde, a widely used molluscicide, is an emerging contaminant in water sources due to its persistence and high solubility [1-4]. It exceeds the EU Drinking Water Directive's limit and poses environmental and health risks [2]. However, current water treatment

---

\* Corresponding author: [farrahaini@unimap.edu.my](mailto:farrahaini@unimap.edu.my)

technologies struggle with metaldehyde contamination and ineffective at removing it, necessitating new solutions [4].

Various adsorbents have been studied for metaldehyde removal, including biological activated carbon [5], functionalized mesoporous silicas [6], and ion-exchange resins [7]. Biochar, particularly from oil palm and rice husk, has shown promise due to its cost-effectiveness, efficiency, and scalability [8,9]. Biochar, a carbon-rich material from biomass pyrolysis, is gaining attention as a potential adsorbent. It has a large specific surface area, negative surface charges, and various pore characteristics [10]. Oil palm and rice husk biochar are commonly studied for their adsorption properties.

This study aims to investigate the use of oil palm kernel biochar and also rice husk biochar for metaldehyde adsorption. Through batch adsorption experiments, the study will evaluate the efficacy of these biochars in removing metaldehyde, leading to the advancement of effective and sustainable remediation techniques.

## **2 Materials and methods**

### **2.1 Preparation of biochar**

Rice husk and oil palm kernels were collected, washed, and dried. They were placed in a porcelain basin and subjected to a controlled pyrolysis process in a furnace for 4 hours at 600°C. After cooling naturally, the resulting biochar was removed, washed, dried, and stored in an airtight container for future use.

### **2.2 Preparation of metaldehyde stock solution**

A metaldehyde stock solution was prepared by dissolving 0.1g of metaldehyde powder in 100mL of methanol, resulting in a 1000µg/L solution. This solution can be stored between 1°C and 10°C for up to a year. Different concentrations of metaldehyde were prepared using deionized water. A standard curve was established using a series of dilutions from the stock solution, covering a range of concentrations. Each dilution was mixed thoroughly to ensure homogeneity.

### **2.3 Characterization of biochar**

Biochar samples were prepared and analyzed using Scanning Electron Microscopy (SEM) to study their surface and structure. The samples were dehydrated, fixed, coated with platinum, and imaged under optimized SEM parameters. The resulting images were used to characterize the biochar's morphology and surface features. The Brunauer-Emmett-Teller (BET) method was used to analyze the biochar. The biochar sample was sieved, degassed, and then subjected to gas adsorption at different pressures. An adsorption isotherm was obtained and used to calculate the biochar's specific surface area and other properties. This method provided valuable insights into the biochar's porosity and surface area.

### **2.4 Batch adsorption**

The study observed the effects of initial metaldehyde concentration, contact time, and adsorbent dosage on its adsorption by biochar. Biochar samples were mixed with metaldehyde solutions of varying concentrations and shaken for different periods. The remaining metaldehyde concentration was measured using UV-Vis. This process was repeated in triplicate for accuracy.

## 2.5 Isotherm and kinetics of adsorption

This study uses the Langmuir and Freundlich isotherms and pseudo first and second order kinetic models to analyze metaldehyde adsorption behavior on rice husk and oil palm biochar. The equations for each model are as follows:

**Table 1.** Mathematical models for isotherm and kinetic.

Model	Equation
Langmuir	$q_e = \frac{q_m \cdot K \cdot C_e}{1 + K \cdot C_e}$
Freundlich	$\log q_e = \log k_f + \frac{1}{n} \cdot \log C_e$
First-order Kinetic	$\log(q_e - q_t) = \log q_e - \frac{k_1}{2.303} \cdot t$
Second-order Kinetic	$q_t = \frac{q_e^2 \cdot k_2 \cdot t}{1 + q_e \cdot k_2 \cdot t}$

## 3 Results and Discussion

### 3.1 Characterization of oil OPKB and RHB by SEM

The SEM analysis of both oil palm kernel biochar (OPKB) and rice husk biochar (RHB) exhibited comparable pore structures. Fig.1 shows the images of OPKB and RHB under SEM, revealing highly porous surfaces with diverse pore sizes and shapes. Macropores, mesopores, and micropores were observed in both biochars. Fig.1(B) shows OPKB with macropores (>50nm) of irregular shapes, mesopores (2-50nm) with regular shapes, and abundant micropores (<2nm) forming intricate networks. These pore structures enhance the adsorption potential of OPKB. Similarly, Fig.1(D) shows RHB with a distinct, highly porous surface and uniformly distributed pores forming an interconnected network. Each biochar has irregular pore structures and rough surfaces, facilitating adsorption. Macropores enable rapid mass transfer, mesopores provide additional adsorption sites, and micropores contribute to the overall surface area and adsorption through interactions with organic molecules. OPKB exhibited a higher active site for adsorption, like findings by Tang et al. [11]. Hidayat et al. [12] demonstrated that rice husk biochar has a larger pore size, indicating high porosity and adsorption capacity for various pollutants.

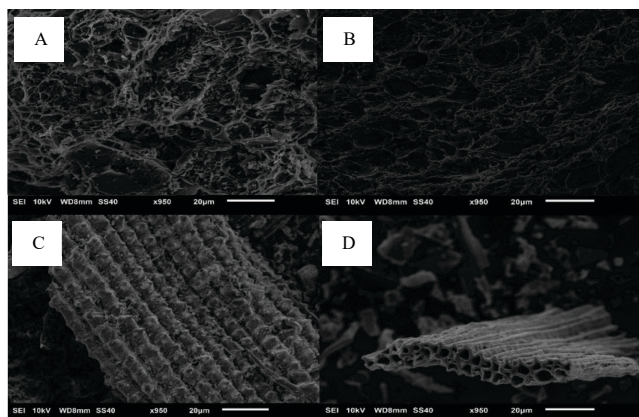


**Fig. 1.** SEM image of (A) raw oil palm kernel, (B) oil palm kernel biochar (C) raw rice husk, and (D) rice husk biochar.

### 3.2 Characterization of oil palm kernel biochar and rice husk biochar by BET

The BET surface area of OPKB was 123.08m<sup>2</sup>/g, with a pore volume of 0.43cm<sup>3</sup>/g and a porosity of 0.95. RHB had a BET surface area of 72.49m<sup>2</sup>/g, a pore volume of 0.23cm<sup>3</sup>/g, and a porosity of 0.94. Table 2 summarizes these BET results, showing that each biochar has high specific surface areas and wide pore size distributions. The primary difference is the higher specific surface area of OPKB, likely due to differences in feedstock material. The carbon content of feedstock affects biochar properties, with carbon-rich materials producing biochar with greater surface areas through carbonization.

Aprilia et al. [13] reported rice husk carbon content between 10%-15%, and Lala et al. [14] noted variations up to 26.69%. Affam et al. [15] indicated a high carbon concentration in oil palm kernels, with lignocellulosic content around 36.4%-47.3%, suggesting a higher BET surface area. Despite similar pore characteristics, including mesopores, OPKB and RHB differ in specific surface areas and pore volumes. Burachevskaya et al. [16] noted that RHB has a smaller BET surface area than other biochars. However, Hidayat et al. [12] reported that RHB has a larger pore volume and size compared to coconut fiber biochar, implying potential variations in BET surface areas among different biomass sources.

**Table 2.** Summary of BET results for oil palm kernel biochar and rice husk biochar.

Type of biochar	Bet surface area (m <sup>2</sup> /g)	Total Pore Volume (cm <sup>3</sup> /g)	Porosity
Oil palm kernel biochar (OPKB)	123.08	0.43	0.95
Rice husk biochar (RHB)	72.49	0.23	0.94

### 3.3 Batch adsorption of metaldehyde

The adsorption of metaldehyde using OPKB and RHB was studied under varying initial concentrations of metaldehyde. The results for this batch adsorption study are shown in Fig.2, Fig.2(A) shows the graph of the effect of the initial concentration on adsorption efficiency for both types of biochar. The results indicated that the percentage of adsorption efficiency of metaldehyde by OPKB increased with increasing initial concentrations of metaldehyde. The highest percentage of adsorption efficiency with 94.1% was observed for OPKB at an initial concentration of 500µg/L. The percentage of adsorption efficiency of RHB also increased with increasing initial concentrations of metaldehyde, but to a lesser extent than OPKB. The highest percentage of adsorption efficiency with 92.8% was observed for RHB at an initial concentration of 100µg/L. The results of this study suggest that the adsorption of metaldehyde by biochar is a surface-area-controlled process. This means that the amount of metaldehyde that can be adsorbed by biochar is limited by the surface area of the biochar. As the initial concentration of metaldehyde increases, more of the biochar surface is available for adsorption, resulting in a higher percentage of adsorption efficiency.

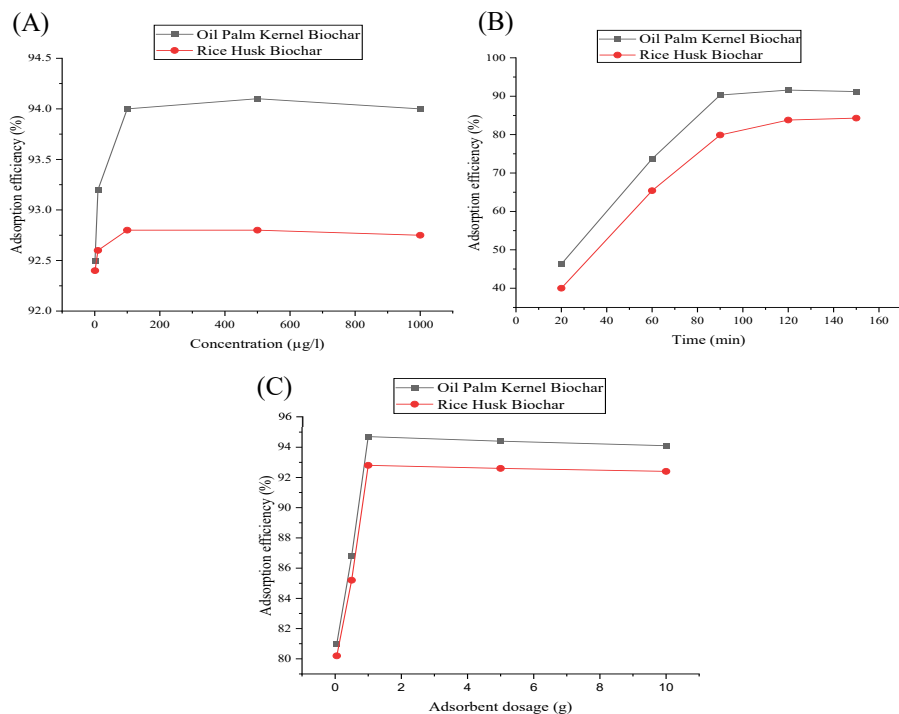


**Fig. 2.** The graph of (A) the effect of initial concentration of metaldehyde on adsorption efficiency, (B) the effect of contact time on the percentage of adsorption efficiency, and (C) the effect of adsorbent dosage on the percentage of adsorption efficiency.

The superior adsorption efficiency of OPKB can be attributed to its unique properties, including a larger surface area, a greater pore volume, and possibly its chemical composition. These factors contribute to the higher availability of adsorption sites, facilitating the interactions between the molecules of metaldehyde and the biochar surface [17]. The higher adsorption efficiency observed for OPKB across the range of initial concentrations indicates its robust adsorption capability and suitability for removing metaldehyde from water. The slightly lower adsorption efficiencies observed for RHB may be attributed to its comparatively smaller surface area and lower pore volume as compared to OPKB. However, despite the slightly lower efficiency, RHB still demonstrated significant adsorption performance, highlighting its potential as an alternative adsorbent for metaldehyde removal. These findings suggest that the initial concentration of metaldehyde significantly influences the adsorption efficiency of both biochars. The results indicate that OPKB exhibits higher adsorption efficiency compared to RHB across varying initial concentrations.

The next parameter is to evaluate the impact of varying contact times on the adsorption efficiency of OPKB and RHB. As illustrated in Fig.2(B), OPKB demonstrated superior performance at all tested contact times, achieving an efficiency of 91.6% after 120 minutes. In contrast, RHB reached its peak efficiency of 84.3% at a slightly longer contact time of 150 minutes. These observations suggest that the adsorption process is kinetically controlled, with efficiency improving over time until a saturation point is reached. The principles of adsorption kinetics, which dictate that the speed of adsorption is determined by the frequency of molecules reaching the surface and the percentage of those molecules that are adsorbed [18], align with these findings. Additionally, prior research has shown that the efficiency of adsorption initially rises significantly over time, but the rate of increase slows down between

60 and 120 minutes. Eventually, a state of relative equilibrium is achieved, reflecting a balance between the solid phase under investigation and the solution phase [19].

Adsorbent dosage studies (Fig.2(C)) revealed that OPKB had the highest efficiency at various dosages, with a peak of 94.7% at 1g/L, compared to RHB's 92.8% at the same dosage. OPKB's higher surface area and wider pore size distribution likely account for its superior performance [20]. The effectiveness of an adsorbent in capturing contaminants is closely related to its surface area and pore size distribution. Textural characteristics such as surface area, pore volume, average pore diameter, and pore-size distribution play a crucial role in adsorption processes [21]. This aligns with the observation that OPKB, with its higher surface area and wider pore size distribution, outperformed RHB in adsorption efficiency [20]. The ability of OPKB to reach a peak efficiency of 94.7% at 1g/L can be directly correlated with its favorable textural properties.

### 3.4 Isotherm and kinetics of adsorption

The adsorption of metaldehyde onto OPKB and RHB was investigated using Langmuir and Freundlich isotherms, as tabulated in Table 3. The Langmuir isotherms for OPKB and RHB displayed high  $R^2$  values of 0.988 and 0.986, respectively, indicating a strong fit of the Langmuir model to the data, suggesting a significant relationship between the amount adsorbed and the metaldehyde content [22]. However, the Freundlich isotherms for OPKB and RHB exhibited even higher  $R^2$  values of 0.999 and 0.998, respectively, indicating a superior fit compared to the Langmuir model. This preference for the Freundlich model suggests a more robust correlation, pointing towards a heterogeneous adsorption surface with multilayer adsorption and non-uniform adsorption energy distribution [23].

**Table 3.** The Isotherm and Kinetics parameters of OPKB and RHB.

	Models	Parameters	OPKB	RHB
Isotherm	Langmuir	$R^2$	0.988	0.986
	Freundlich	$R^2$	0.999	0.998
Kinetics	Pseudo-first order	$R^2$	0.991	0.970
	Pseudo-second order	$R^2$	0.997	0.996

Regarding the kinetics of metaldehyde adsorption, both pseudo-first-order and pseudo-second-order models were employed. The pseudo-first-order model, characterized by a linear relationship between  $\log(q_e - q_t)$  and time, demonstrated  $R^2$  values of 0.991 for OPKB and 0.970 for RHB, indicating physisorption involving weak van-der-Waals interactions, which are reversible in nature [24]. Conversely, the pseudo-second-order model, depicted by a linear relationship between  $t/q_t$  and time, suggested chemisorption with  $R^2$  values of 0.997 for OPKB and 0.996 for RHB. This model implies the formation of a chemical bond between the adsorbate and the adsorbent, highlighting adsorption as the rate-limiting step. The higher  $R^2$  values associated with the pseudo-second-order model suggest that chemisorption is the predominant mechanism for metaldehyde adsorption onto both biochars [25].

## 4 Conclusion

The study compared the adsorption of metaldehyde by OPKB and RHB. OPKB showed higher adsorption due to its unique structure and composition. Both Langmuir and Freundlich isotherms fit the data well, with the Freundlich model slightly better. The adsorption process followed similar kinetic models for both biochars, with the pseudo-second-order model being more appropriate. Overall, these findings have the potential to contribute to the development

of more efficient and effective technologies for removing metaldehyde from contaminated water sources. By understanding how various kinetic models explain this process over time, researchers can make more accurate predictions regarding the amount of time required to remove a specific amount of metaldehyde from solution using a particular type of adsorbent material. This knowledge can then be used to enhance remediation procedures and reduce the negative impacts of pesticide contamination on the surrounding ecosystem.

The authors acknowledge UniMAP for supporting this research. This research was funded by the Ministry of Higher Education Malaysia - FRGS/1/2020/TK0/UNIMAP/02/104.

## References

1. Z. Li, J. Li, Z. Guo, L.C. Campos, *Environ. Sci.: Water Res. Technol.* **6**, 1432 (2020)
2. G.D. Castle, G.A. Mills, A. Gravell, A. Leggatt, J. Stubbs, R. Davis, G.R. Fones, *Environ. Monit. Assess.* **191** (2019)
3. G.D. Castle, G.A. Mills, A. Bakir, A. Gravell, M. Schumacher, K. Snow, G.R. Fones, *Environ. Sci.: Process. Impacts* **20**, 1180 (2018)
4. A.M. Saad, S.W. Ismail, F.A. Dahalan, *JCEST*, **8**, 108 (2017)
5. C.A. Rolph, B. Jefferson, F. Hassard, R. Villa, *Environ. Sci.: Water Res. Technol.* **4**, 1543 (2018)
6. B. Tao, A.J. Fletcher, *Sep. Purif. Technol.* **124**, 195 (2014)
7. L.L. Tang, M.A. Denardo, C. Gayathri, R.R. Gil, R. Kanda, T.J. Collins, *Environ. Sci. Tech.* **50**, 5261 (2016)
8. R. Busquets, O.P. Kozynchenko, R.L. Whitby, S.R. Tennison, A.B. Cundy, *Water Res.* **61**, 46 (2014)
9. A. Ferino-Pérez, J.J. Gamboa-Carballo, Z. Li, L.C. Campos, U. Jáuregui-Haza, *J. Mol. Graphics Modell.* **90**, 94 (2019)
10. M. Ahmadvand, J. Soltani, S.E.G. Hashemi, M. Varavipour, *Environmental Health Engineering and Management* **5**, 67 (2018)
11. J. Tang, B. Xiang, Y. Li, T. Tan, Y. Zhu, *Front. Chem.* **10**, 1 (2022)
12. B. Hidayat, A. Rauf, T. Sabrina, A. Jamil, *Journal of Asian Scientific Research* **8**, 293 (2018)
13. S. Aprilia, B. Arifin, N. Arahman, A.A. Abubakar, A.V. Wicaksono, D. Bakhtiar, *Rasayan J. Chem.* **12**, 994 (2019)
14. M.A. Lala, O.A. Adesina, O.J. Odejebi, J.A. Sonibare, *Niger. J. Phys.* **4**, 954 (2022)
15. A.C. Affam, B.A. Chundi, W.C. Chung, *IOP Conf. Ser. Earth Environ. Sci.* **1135** (2023)
16. M. Burachevskaya, T. Minkina, T. Bauer, I. Lobzenko, A. Fedorenko, M. Mazarji, S. Sushkova, S. Mandzheva, A. Nazarenko, V. Butova, M.H. Wong, V. D. Rajput, *Sci. Rep.* **13**, 2020 (2023)
17. J.O. Eduah, E.K. Nartey, M.K. Abekoe, S.W. Henriksen, M.N. Andersen, *Environ. Technol. Innovation* **17**,100572(2020)
18. M. Wulandari, N. Syamsudin, S.A.S. Sulaiman, *Indones. J. Chem.* **22**, 1612 (2022)
19. H. Barkhor, M.A. Nasser, N. Nasseh, A.Z. Moghaddam, *Biomass. Convers. Biorefin.* (2024)

20. C.O. Ania, B. Cabal, C. Pevida, A. Arenillas, J.B. Parra, F. Rubiera, *J.J. Pis, Appl. Surf. Sci.* **253** (2007)
21. C.S. Ion, M. Bombos, R. Doukeh, G. Vailievici, V. Matei, *Rev. Chim.* **69**, 3439 (2018)
22. D. Hsu, C. Lu, T. Pang, Y. Wang, G. Wang, *Applied Sciences* **9**, 5249 (2019)
23. S. Tayibi, F. Monlau, N.E. Fayoud, E. Abdeljaoued, H. Hannache, Y. Zeroual, A. Oukarroum, A. Barakat, *ACS Omega* **6**, 159 (2021)
24. H. Park, J. Kim, Y.G. Lee, K. Chon, *Water* **13**, 1495 (2021)
25. Z. Mahdi, A.E. Hanandeh, Q. Yu, *MATEC Web Conf.* **120**, 05005 (2017)